Seismic Time-Lapse Imaging using Interferometric Least-Squares Migration

Mrinal Sinha and Gerard Schuster, King Abdullah University of Science and Technology

SUMMARY

One of the problems with 4D surveys is that the environmental conditions change over time so that the experiment is insufficiently repeatable. To mitigate this problem, we propose the use of interferometric least-squares migration (ILSM) to estimate the migration image for the baseline and monitor surveys. Here, a known reflector is used as the reference reflector for ILSM. Results with synthetic and field data show that ILSM can eliminate artifacts caused by non-repeatability in time-lapse surveys.

INTRODUCTION

Water-layer velocity is known to vary during an ongoing survey because of environmental factors such as seasonal temperature and salinity. These deviations lead to uncertainty in the estimation of the water-layer velocity, which can lead to image distortion similar to that of static errors in land data. In addition tidal variations will introduce statics shifts into marine data. Therefore, repeatable surveys is a challenge for monitoring of reservoirs.

To overcome this problem, Rickett and Lumley (1998) used cross-equalization to ensure repeatability over different surveys. Cross-equalization is a processing workflow devised for post-stack seismic data which corrects for differential statics, NMO velocity, source wavelet effects and also balances the amplitude differences for the baseline and monitor surveys. Bakulin and Calvert (2004) proposed VSP data as natural Green's functions to redatum the data to a datum below the complex overburden. This method, in theory, overcomes the non-repeatability caused by the source-side statics.

Zhou et al. (2006) introduced the concept of interferometric migration to mitigate the defocusing due to the statics contained in the data. In this method they shifted the data by the traveltimes of the picked reference reflections. This time-shift can also be automatically computed by cross-correlating the original trace with the trace windowed around the reference reflection. This procedure is carried out for all the traces. This nearly cancels out the phase associated with the common raypaths above the reference interface for small source-receiver offsets. It also approximately redatums the data to the reference interface without a known velocity model. We can avoid errors due to uncertainty in estimation of the water-layer velocity and also ensure a fixed geometry by redatuming the data to this known reference reflector, thereby improving the repeatability. Interferometric least-squares migration, which is an extension of interferometric migration, gives better balanced amplitudes.

This paper is organized into four sections. After the introduction, the second section describes the theory of interferometic least-squares migration. The objective function is defined and the associated gradient is derived for use in a conjugate gradient method. Numerical results are presented in the next section, and the conclusions are in the last section.

THEORY

Let the recorded trace in the frequency domain be denoted by $\tilde{D}(\mathbf{g}|\mathbf{s})$ and the predicted trace be denoted by $D(\mathbf{g}|\mathbf{s})$ for a source at $\mathbf{s}$ and geophone at $\mathbf{g}$. Let $D(\mathbf{g}|\mathbf{s})_{ref}$ denote the trace that is windowed around a reference reflection event as illustrated in Figure 1. To estimate the crosscorrelogram $\Phi(\mathbf{g}|\mathbf{s})$, the windowed reference reflections in the data are temporally crosscorrelated with the recorded traces. In the frequency do-
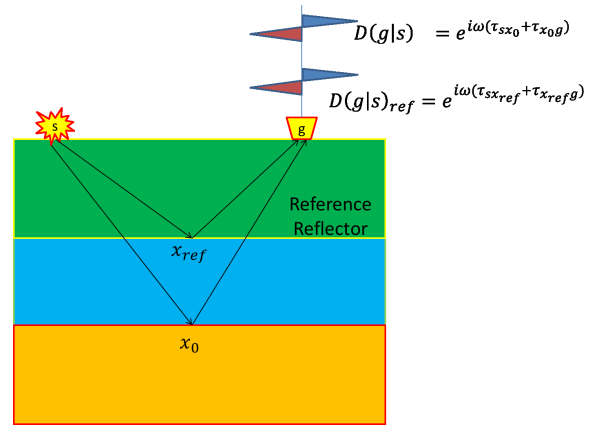
Figure 1: A crosscorrelogram is obtained by cross-correlating a recorded trace with the same trace windowed around the reference reflection.

main, crosscorrelation is equivalent to the conjugated product of spectra

$$\Phi(\mathbf{g}|\mathbf{s}) = D(\mathbf{g}|\mathbf{s})D^*(\mathbf{g}|\mathbf{s})_{ref}, \tag{1}$$

which removes the 2-way propagation time from the surface to the reflector for near-offset traces. For example, denote the 2-way propagation time to the reference interface as $\tau_{\mathbf{s}\mathbf{x}_{ref}} + \tau_{\mathbf{x}_{ref}\mathbf{g}}$ so that $D(\mathbf{g}|\mathbf{s})_{ref} = e^{i\omega(\tau_{\mathbf{s}\mathbf{x}_{ref}} + \tau_{\mathbf{x}_{ref}\mathbf{g}})}$. If the reflection data from a deeper interface is given as $D(\mathbf{g}|\mathbf{s}) = e^{(\tau_{\mathbf{s}\mathbf{x}_0} + \tau_{\mathbf{x}_0\mathbf{g}})}$ then $D(\mathbf{g}|\mathbf{s})D(\mathbf{g}|\mathbf{s})^*_{ref} = e^{(\tau_{\mathbf{s}\mathbf{x}_0} + \tau_{\mathbf{x}_0\mathbf{g}} - \tau_{\mathbf{s}\mathbf{x}_{ref}} - \tau_{\mathbf{x}_{ref}\mathbf{g}})}$. Thus, the deep reflection data have been naturally redatumed to the reference reflector without knowing the velocity model. However, the implicit assumption is that the reflection rays for the reference reflection coincide with a portion of the rays associated with the deep reflection. Similarly, the observed crosscorrelogram $\tilde{\Phi}(\mathbf{g}|\mathbf{s})$ can be obtained by the crosscorrelation of recorded traces with the observed reference reflection traces. The goal is to find the reflectivity model which maximizes the normalized dot product of the observed and predicted crosscorrelograms.

This can be written as (Routh et al., 2011; Zhang et al., 2013; Dutta et al., 2014),

$$\varepsilon = -\sum_{\omega}\sum_{s}\sum_{g} \frac{\Phi(\mathbf{g}|\mathbf{s})^{*}}{||\Phi(\mathbf{g}|\mathbf{s})||} \frac{\tilde{\Phi}(\mathbf{g}|\mathbf{s})}{||\tilde{\Phi}(\mathbf{g}|\mathbf{s})||}, \tag{2}$$

where we call this an interferometric objective function. The gradient of equation 2 with respect to the perturbation in slowness is

$$\frac{\partial \varepsilon}{\partial s(\mathbf{x})} =$$
$$-\sum_{\omega}\sum_{s}\sum_{g} \frac{1}{||\Phi(\mathbf{g}|\mathbf{s})||} \frac{\partial \Phi}{\partial s(\mathbf{x})} [w(\mathbf{g}|\mathbf{s}) \frac{\Phi(\mathbf{g}|\mathbf{s})}{||\Phi(\mathbf{g}|\mathbf{s})||} - \frac{\tilde{\Phi}(\mathbf{g}|\mathbf{s})}{||\tilde{\Phi}(\mathbf{g}|\mathbf{s})||}], \tag{3}$$

where $w(\mathbf{g}|\mathbf{s})$ is the weight given by $w(\mathbf{g}|\mathbf{s}) = \frac{\Phi(\mathbf{g}|\mathbf{s})}{||\Phi(\mathbf{g}|\mathbf{s})||} \cdot \frac{\tilde{\Phi}(\mathbf{g}|\mathbf{s})}{||\tilde{\Phi}(\mathbf{g}|\mathbf{s})||}$, which emphasizes the phase mismatch between the observed and the predicted crosscorrelograms. If two crosscorrelograms match perfectly then $w(\mathbf{g}|\mathbf{s}) = 1$.

Substituting the expression for predicted crosscorrelograms in equation 1 into equation 3 gives

$$\frac{\partial \varepsilon}{\partial s(\mathbf{x})} = - \overbrace{\frac{\partial D^{*}(\mathbf{g}|\mathbf{s})}{\partial s(\mathbf{x})}}^{\textit{Migration kernel}}$$
$$\overbrace{\frac{1}{||\Phi(\mathbf{g}|\mathbf{s})||} D(\mathbf{g}|\mathbf{s})_{ref} [w(\mathbf{g}|\mathbf{s}) \frac{\Phi(\mathbf{g}|\mathbf{s})}{||\Phi(\mathbf{g}|\mathbf{s})||} - \frac{\tilde{\Phi}(\mathbf{g}|\mathbf{s})}{||\tilde{\Phi}(\mathbf{g}|\mathbf{s})||}]}^{\textit{Weighted crosscorrelogram residual}}, \tag{4}$$

where the Fréchet derivative $\frac{\partial D(\mathbf{g}|\mathbf{s})}{\partial s(\mathbf{x})}$ is given by Luo and Schuster (1991) as

$$\frac{\partial D(\mathbf{g}|\mathbf{s})}{\partial s(\mathbf{x})} = 2\omega^{2} s(\mathbf{x}) G(\mathbf{g}|\mathbf{x}) G(\mathbf{x}|\mathbf{s}). \tag{5}$$

Equation 4 says that the interferometric gradient (or migration image) is formed by smearing the weighted crosscorrelogram residual along the associated migration ellipses. Detailed analysis of the gradient using high frequency asymptotic Green's functions can be found in Sinha and Schuster (2015).

The next subsection describes the workflow of the method.

Workflow

- Define a reference reflector in the reflectivity model and window the corresponding reference reflection in the observed data.

- Crosscorrelate the observed data with observed reference reflection data to get the observed crosscorrelogram. Now calculate the interferometric residual in equation 4.

- Calculate the gradient $\mathbf{g}^{k+1}$ in equation 4 and update the search direction $\mathbf{d}^{k}$ using the conjugate gradient method (Nocedal and Wright, 2006)

$$\mathbf{d}^{k+1} = -\mathbf{g}^{k+1} + \beta \mathbf{d}^{k}, \tag{6}$$

where β is calculated using the Fletcher-Reeves formula

$$\beta = \frac{(\mathbf{g}^{k+1}, \mathbf{g}^{k+1})}{(\mathbf{g}^{k}, \mathbf{g}^{k})}. \tag{7}$$

- Compute the step length α by a line-search method.

- Update the migration image $\mathbf{m}^{k+1}$ by

$$\mathbf{m}^{k+1} = \mathbf{m}^{k} + \alpha \mathbf{d}^{k+1}. \tag{8}$$

- Calculate the new predicted crosscorrelogram using equation 1.

The migration images calculated from baseline and monitor surveys are then subtracted to obtain the time-lapse migration image.

The effectiveness of ILSM in mitigating the errors caused due to non-repeatability between different surveys of a 4D survey is illustrated with numerical examples.

NUMERICAL EXAMPLE

To test the application of ILSM to 4D data, a fixed-spread acquisition geometry is used for both the baseline and the monitor surveys. The velocity model used for generating the data and imaging are the same for the baseline survey as shown in Figure 2. The reflectivity model used for generating the data is shown in Figure 3(a), the shallow reflector can be thought of as the sea-bottom and the second reflector is taken to be the top interface of a reservoir. The velocity model used for generating the monitor data is shown in Figure 4(a). It contains a low-velocity anomaly in the water layer which generates static shifts in the data and hampers the repeatability of the time-lapse survey. The migration velocity model for the monitor survey is shown in Figure 4(b). The missing low-velocity anomaly in the migration velocity model can be thought of as an uncertainty in estimation of water-layer velocity. The net change in the reflectivity over the course of the two surveys is shown in Figure 3(b), where only the reservoir reflectivity has changed and the sea-bottom remains the same. Also, the source and receiver positions of the monitor survey vary randomly and introduce random static shifts in the data. These statics can be thought of as the effect of varying tidal conditions from one survey to another.

LSM and ILSM (sea-bottom is used as reference reflector) are used to obtain the migration images for both the baseline and monitor surveys, and the results are shown in Figures 5 and 6. The time-lapse image obtained by ILSM shows reflectivity changes at the reservoir reflector and is immune to the time-lapse statics. In contrast, the LSM image mispositions the reservoir reflector because it is affected by the time-lapse statics.

Next we apply ILSM to time-lapse data from the Norne field. The baseline survey was conducted in 2001 and the monitor survey was collected in the year 2006. A 2-D line was selected for the ILSM test. The input is post-stack data comprised of 1001 traces spaced at an interval of 12.5 m. The
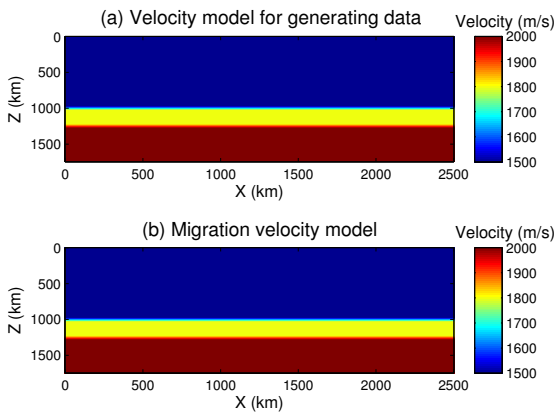
Figure 2: (a) Velocity model used for generating the data and (b) migration velocity model for the baseline survey.
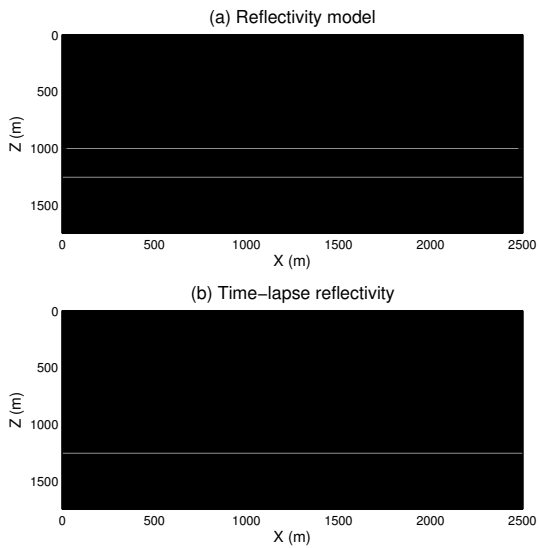
Figure 3: (a) Reflectivity model used for generating the data for baseline survey. (b) Time-lapse reflectivity, the difference between the monitor and base survey reflectivity distributions. The sea-bottom remains same hence gets canceled out.
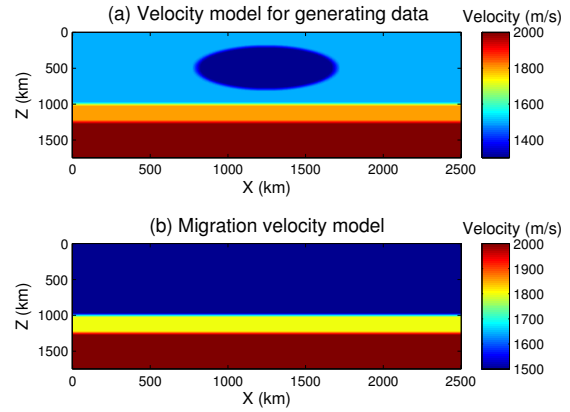
Figure 4: (a) Velocity model used for generating the data and (b) migration velocity model for the monitor survey.
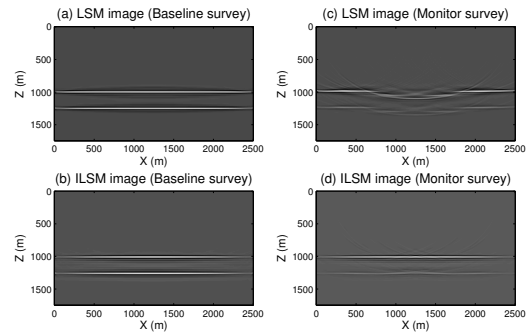
Figure 5: (a) LSM image and (b) ILSM image for the baseline survey. (c) LSM image and (d) ILSM image for the monitor survey.
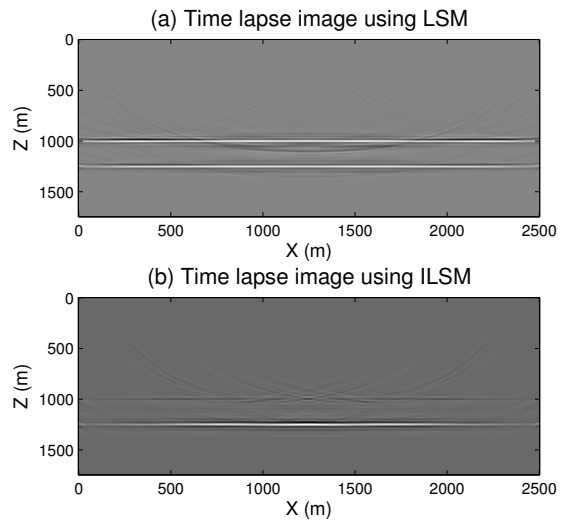
Figure 6: Time-lapse images using a) LSM and b) ILSM.

data provided was cross-equalized. Therefore this dataset does not suffer greatly from non-repeatability. The interval velocity was used for migration and the sea-bottom is chosen as the reference reflector. The LSM and ILSM images are shown in Figures 7 (a) and (b) respectively. The LSM image shows the reservoir changes sufficiently well, however we see some small changes close to the sea-bottom. On comparison with the ILSM images we see the changes close to the sea-bottom are minimized. Red arrows in Figure 7 show one of the areas where time-lapse changes close to the sea-bottom are better eliminated by ILSM. Zoomed views of the black and blue boxes in Figure 7 are shown in Figure 8. Figures 8(a) and (b) show stronger amplitudes in the reservoir region (marked by black arrow) for the time-lapse image obtained by ILSM. Figures 8(c) and (d) show the zoomed view of the blue box where we can see that the marked reflectors are better delineated in the ILSM image.

Figure 8: Zoom views of the black and blue boxes in Figure 7. (a) Time-lapse image estimated using LSM and ILSM (black box). (c) Time-lapse image estimated using LSM and (d) ILSM (blue box).
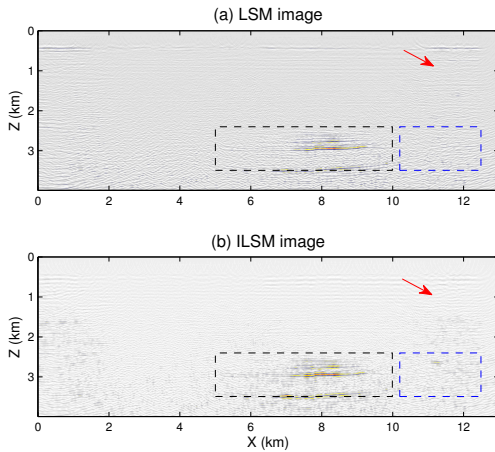
Figure 7: Time-lapse image estimated using (a) LSM and (b) ILSM.

CONCLUSIONS

ILSM has the potential to mitigate ill-effects of the repeatability errors on seismic time-lapse images. ILSM approximately redatums the data to a fixed reference interface which leads to improved repeatability between the baseline and monitor surveys. Results with synthetic and field data show that by choosing a reference reflector close to the target area, reservoir changes can be mapped with better accuracy in the presence of repeatability errors.

ACKNOWLEDGEMENTS